Accurate Indoor Localization by Combining IEEE 802.11 g/n/ac WiFi-Systems with Strapdown Inertial Measurement Units

Kristoph Keunecke[1], Gerd Scholl[2]
[1]Electrical Measurement Engineering, Helmut-Schmidt-University, Hamburg, Germany, kristoph.keunecke@hsu-hh.de
[2]Electrical Measurement Engineering, Helmut-Schmidt-University, Hamburg, Germany, gerd.scholl@hsu-hh.de

Abstract—WiFi signals delivered by a radio frequency (RF) transceiver unit and a strapdown inertial measurement unit (IMU) are combined to realize a highly accurate navigation/localization system. The performance of this approach is evaluated by a system simulation. Mobile station (MS) motion data and WiFi range estimates are superimposed by real-world noise signals. Both sensor signals, the noisy WiFi signal and the motion signal delivered by the IMU are fused employing an extended Kalman filter (EKF). The simulation studies presented in this article show that WiFi-IMU-EKF navigation filter can achieve a significant increase in location accuracy compared to stand-alone IMU or WiFi solutions and that the integrated approach may provide a cost-effective and accurate system for many indoor location systems.

Index Terms—inertial navigation system, indoor localization, WiFi, zero-velocity updates.

I. Introduction

In order to realize a high performance indoor localization system we coupled an inertial measurement unit (IMU) based on micro-machined triaxial inertial accelerometers and gyroscopes with a WiFi-system as aiding reference. The redundant position information is frequently fed into an extended Kalman filter (EKF) to compensate sensor biases, to update velocity errors and to compute optimal estimates of the IMU position and orientation.

To avoid complex measurement setups in an early development phase this article evaluates the navigational performance of a hybrid WiFi-IMU-EKF approach driven by simulated motion data of a mobile station (MS). Based on a 2D-reference path IMU sensor data and WiFi range estimations are generated by adding random noise signals according to IMU sensor specifications and WiFi location errors carried out in prior investigations [1]-[5]. These synthesized data are input parameters for the WiFi-IMU-EKF navigation filter.

With simulations presented in [1][2] we have shown that with moderate modifications of current WiFi chip sets and employing algorithms already known from OFDM (Orthogonal Frequency-Division Multiplexing) based RADAR (Radio Detection And Ranging) systems an improved location accuracy compared with an Received Signal Strength Indicator (RSSI) approach can be achieved. It is assumed that the WiFi-IMU-EKF navigation algorithm is fed by Time Difference of Arrival (TDOA) range estimates delivered by a WiFi g/n/ac infrastructure.

The determination of the position of an object in 3D-space using IMU data is based on double integrating acceleration data and removing effects of the earth's rotation and gravity. Generally, the sensor signal is superimposed by several noise sources such as white noise and bias instabilities. So, even in de-facto standstill zero-velocity is actually never reached and the position error increases rapidly over time. To improve IMU navigation performance some zero-velocity detection (ZVD) tests were evaluated in [3]-[5] to discriminate the MS motion states motion and standstill by analyzing raw IMU sensor data. ZVD tests were evaluated in a real-world robotic indoor localization scenario [5] in which a significant increase in location accuracy could be achieved. Hence, the MS motion state delivered by ZVD tests is an additional input parameter for the WiFi-IMU-EKF.

This article is organized as follows. A short overview of inertial navigation is given in Section II. In Section III the WiFi-IMU-EKF navigation filter is presented fusing WiFi and IMU observations. The simulation model for development and testing the navigation algorithm is described in Section IV. In Section V the WiFi-IMU-EKF navigation algorithm is comprehensively discussed. To demonstrate the improvement that can be achieved with the combined WiFi-IMU-EKF approach in comparison the navigation results of the WiFi-only, IMU-only and outdoor scenario paths were calculated. Concluding remarks are given in the final Section VI.

II. Inertial Navigation

Inertial navigation means the determination of a MS path by an appropriate interpretation of strapdown inertial sensors. Based on Newton's second law of motion the MS will remain in standstill or a uniform motion unless an external force is applied. If acceleration is detected and the sensor signals are integrated the change in velocity and position of the MS with respect to an initial condition can be calculated. Therefore, an IMU contains at least a combination of a triaxial micro-machined accelerometer and a triaxial gyroscope. The measured sensor signal has to be rotated from the body frame (BF) to the navigation frame. To describe locations, motions

ISBN 978-3-8007-3585-3

and orientations on the earth's surface often the local level frame (LLF) is used defining a right-handed orthogonal coordinate system such that the x-axis points eastwards, the y-axis to the north and the z-axis upwards building an east-north-up (ENU) system. With angles φ_x, φ_y and φ_z around the x/y/z-axis the BF data can be transformed to LLF data by

$$\mathbf{T}_{\mathrm{LLF,k}} = \mathbf{T}_x \cdot \mathbf{T}_y \cdot \mathbf{T}_z\,, \tag{1}$$

in which transformation matrices $\mathbf{T}_{x/y/z}$ are described in [5]. After transformation of the transposed BF data $\mathbf{a}_k = [a_x, a_y, a_z]^T$ the location-dependent gravity $\mathbf{g}_{\mathrm{LLF}}$ and the earth rotation $\boldsymbol{\varepsilon}_{\mathrm{LLF}}$ have to be removed from the acceleration information. In a quasi-stationary environment, e.g. in an indoor area, the navigation equation is given by the first order differential equation

$$\begin{aligned} \boldsymbol{v}_{\mathrm{LLF,k}} = \boldsymbol{v}_{\mathrm{LLF,k-1}} + \left[\mathbf{T}_{\mathrm{LLF,k}}\boldsymbol{a}_k - \mathbf{g}_{\mathrm{LLF}}\right]T_S \\ - 2\boldsymbol{\varepsilon}_{\mathrm{LLF}} \times \frac{\boldsymbol{v}_{\mathrm{LLF,k}} + \boldsymbol{v}_{\mathrm{LLF,k-1}}}{2} T_S \end{aligned} \tag{2}$$

with $\mathbf{v}_{\mathrm{LLF,k}} = [v_{x,\mathrm{LLF,k}}, v_{y,\mathrm{LLF,k}}, v_{z;\mathrm{LLF,k}}]^T$ and k is a running index representing the evolution over time [6][7]. T_S stands for the IMU sampling rate. Hence, the x/y/z-element IMU position is

$$\boldsymbol{s}_k = \boldsymbol{s}_{k-1} + \frac{\boldsymbol{v}_{\mathrm{LLF,k}} + \boldsymbol{v}_{\mathrm{LLF,k-1}}}{2} T_S. \tag{3}$$

III. WiFi-IMU-EKF Navigation Filter

For WiFi- and IMU-sensor data fusion an extended Kalman filter (EKF) [8][9] is used, where the EKF is an approximate description of the nonlinear system behavior linearizing the nonlinear equation.

A. Transition Model

The linearized state transition model

$$\delta\boldsymbol{x}_k = \boldsymbol{F}_k\,\delta\boldsymbol{x}_{k-1} + \mathbf{w}_k \tag{4}$$

describes the error dynamics. Here $\delta\mathbf{x}_k = [\delta\mathbf{s}_k, \delta\mathbf{v}_k, \delta\mathbf{a}_k, \delta\boldsymbol{\varphi}_k, \delta\boldsymbol{\omega}_k]^T$ represents the transposed 15-element vector of error states in the nonlinear system at time position k. $\mathbf{w}_k$ is the Gaussian process noise vector with $E\{\mathbf{w}_k\} = 0$ and $E\{\mathbf{w}_k\,\mathbf{w}_k^T\} = \mathbf{Q}_k$. $E\{\cdot\}$ stands for the expectation. The 15×15 state transition matrix of the error dynamics is given by [6][7]

$$\boldsymbol{F}_k = \begin{bmatrix} \mathbf{I}_{3\times3} & \mathbf{I}_{3\times3}T_S & \mathbf{0}_{3\times3} & \mathbf{0}_{3\times3} & \mathbf{0}_{3\times3} \\ \mathbf{0}_{3\times3} & \mathbf{A}_1 & \mathbf{A}_2\mathbf{T}_{\mathrm{LLF,k}}T_S & -\mathbf{A}_2\boldsymbol{a}_k T_S & \mathbf{0}_{3\times3} \\ \mathbf{0}_{3\times3} & \mathbf{0}_{3\times3} & \mathbf{S}_a & \mathbf{0}_{3\times3} & \mathbf{0}_{3\times3} \\ \mathbf{0}_{3\times3} & \mathbf{0}_{3\times3} & \mathbf{0}_{3\times3} & \mathbf{A}_2 & \mathbf{A}_2\mathbf{T}_{\mathrm{LLF,k}}T_S \\ \mathbf{0}_{3\times3} & \mathbf{0}_{3\times3} & \mathbf{0}_{3\times3} & \mathbf{0}_{3\times3} & \mathbf{S}_\omega \end{bmatrix} \tag{5}$$

with auxiliary matrices $\mathbf{A}_1 = \mathbf{A}_2\,[\mathbf{I} - \boldsymbol{\varepsilon}_{\mathrm{LLF}} \times \mathbf{I}\,T_S]$ and $\mathbf{A}_2 = [\mathbf{I} + \boldsymbol{\varepsilon}_{\mathrm{LLF}} \times \mathbf{I}\,T_S]^{-1}$. $\mathbf{S}_a$ and $\mathbf{S}_\omega$ denote matrices for describing the time-dependent behavior of sensor errors. If no model is available, $\mathbf{S}_a$ and $\mathbf{S}_\omega$ are set to the identity matrix $\mathbf{I}_{3x3}$. Extrapolations have to be made because position and velocity at time k are not available. With time update equations

$$\delta\boldsymbol{x}_k^- = \boldsymbol{F}_k\,\delta\boldsymbol{x}_{k-1} \tag{6}$$

and

$$\boldsymbol{P}_k^- = \boldsymbol{F}_{k-1}\,\boldsymbol{P}_{k-1}\boldsymbol{F}_{k-1}^T + \boldsymbol{Q}_{k-1} \tag{7}$$

the error state and its error covariance matrix $\mathbf{P}_k$ are projected forward to obtain an a-priori estimate for the next time step indicated by $(\cdot)^-$.

B. Measurement Model

In the measurement model

$$\delta\mathbf{z}_k = \boldsymbol{H}_k\,\delta\boldsymbol{x}_k^- + \mathbf{n}_k \tag{8}$$

the measurement matrix $\mathbf{H}_k$ maps the filtered error state $\delta\mathbf{x}_k^-$ onto the measurement $\delta\mathbf{z}_k$. Again, the measurement error $\mathbf{n}_k$ is assumed to be zero mean and the noise is white and uncorrelated between the error sources, so that $E(\mathbf{n}_k\,\mathbf{n}_k^T) = \mathbf{R}_k$. The measurement

$$\delta\mathbf{z}_k = \left[\boldsymbol{s}_{\mathrm{LLF,IMU,k}} - \boldsymbol{s}_{\mathrm{WiFi,k}}, \mathbf{0}_{1\times12}\right]^T \tag{9}$$

consists of both IMU position $\mathbf{s}_{\mathrm{LLF,IMU}}$ and WiFi reference $\mathbf{s}_{\mathrm{WiFi}}$ at time k, where it is assumed to be a flat area without changes in altitude, i.e. $s_{\mathrm{WiFi,k,z}} = 0$. In this case the 15×15 measurement matrix is

$$\boldsymbol{H}_k = \begin{bmatrix} \mathbf{I}_{3\times3} & \mathbf{0}_{3\times12} \\ \mathbf{0}_{12\times3} & \mathbf{0}_{12\times12} \end{bmatrix}. \tag{10}$$

If the MS is in standstill, zero-velocity, zero-acceleration and zero-angular rate is assumed for the IMU resulting in

$$\begin{aligned} \delta\mathbf{z}_k = \big[\boldsymbol{s}_{\mathrm{LLF,IMU,k}} - \overline{\boldsymbol{s}_{\mathrm{WiFi,k}}},\ \boldsymbol{v}_{\mathrm{LLF,k}} - \mathbf{0}_{1\times3},\ \boldsymbol{a}_k - \mathbf{0}_{1\times3}, \\ \boldsymbol{\varphi}_k - \boldsymbol{\varphi}_{k-1}, \boldsymbol{\omega}_k - \mathbf{0}_{1\times3}\big]^T \end{aligned} \tag{11}$$

and

$$\boldsymbol{H}_k = \begin{bmatrix} \mathbf{I}_{9\times9} & \mathbf{0}_{9\times3} & \mathbf{0}_{9\times3} \\ \mathbf{0}_{3\times9} & \mathbf{0}_{3\times3} & \mathbf{0}_{3\times3} \\ \mathbf{0}_{3\times9} & \mathbf{0}_{3\times3} & \mathbf{I}_{3\times3} \end{bmatrix}. \tag{12}$$

An improved WiFi range estimate $\overline{\boldsymbol{s}_{\mathrm{WiFi,k}}} = \sum_{i=k-n+1}^{n} \boldsymbol{s}_{\mathrm{WiFi,i}}$ is calculated by n observations during a standstill interval.

The measurement update equations

$$\delta\boldsymbol{x}_k^+ = \delta\boldsymbol{x}_k^- + \boldsymbol{K}_k\,(\delta\mathbf{z}_k - \boldsymbol{H}_k\,\delta\boldsymbol{x}_k^-) \tag{13}$$

and

$$\boldsymbol{P}_k^+ = (\mathbf{I} - \boldsymbol{K}_k\,\boldsymbol{H}_k)\,\boldsymbol{P}_k^- \tag{14}$$

are then computed. They are responsible for the feedback information incorporating a new measurement $\delta\mathbf{z}_k$ into the a-priori estimate to obtain an improved a-posteriori estimate $(\cdot)^+$ of $\delta\mathbf{x}_k$ and $\mathbf{P}_k$. Here,

$$\boldsymbol{K}_k = \boldsymbol{P}_k^-\,\boldsymbol{H}_k^T\left(\boldsymbol{H}_k\,\boldsymbol{P}_k^-\,\boldsymbol{H}_k^T + \boldsymbol{R}_k\right)^{-1} \tag{15}$$

denotes the Kalman gain weighting the portion of the measurement residual $\delta\mathbf{z}_k - \mathbf{H}_k\,\delta\mathbf{x}_k^-$ affecting the error state.

ISBN 978-3-8007-3585-3

C. Navigation Error Compensation

At each measurement update the state $\mathbf{x}_k = [\mathbf{s}_k, \mathbf{v}_k, \mathbf{a}_k, \boldsymbol{\varphi}_k, \boldsymbol{\omega}_k]^T$ delivered by the IMU sensor (see Eqs. 2 and 3) are compensated for these errors $\delta\mathbf{x}_k^+$, where the non-bias error terms $\delta\mathbf{s}_k$, $\delta\mathbf{v}_k$ and $\delta\boldsymbol{\varphi}_k$ are set to zero after each estimation cycle. Hence, the result of WiFi-IMU-EKF navigation filter is given by

$$\boldsymbol{c}_k = \boldsymbol{x}_k - \delta\boldsymbol{x}_k^+ , \tag{16}$$

where $\mathbf{s} = [s_x, s_y, s_z]^T = \mathbf{c}_k(1:3)^T$ denotes the estimated x/y/z-MS position

IV. Simulation Model

In order to test the WiFi-IMU-EKF navigation algorithm in a well defined environment, a simulation suite was developed. Our investigations were done with the Xsens IMU MTi-G-700 that was rigidly mounted on a MS. It is assumed that a 70 m by 50 m flat indoor area is equipped with a WiFi infrastructure. Range estimations are delivered to the navigation filter every second, i.e. $f_{S,WiFi} = 1$ Hz, whereas the IMU operates at a sampling rate of $f_{S,IMU} = 100$ Hz. As illustrated in Fig. 1 IMU sensor acceleration $\tilde{\boldsymbol{a}}(t)$ and angular rate $\tilde{\boldsymbol{\omega}}(t)$ as well as the WiFi range estimations $\tilde{\boldsymbol{p}}(t)$ are generated based on the 2D-reference path of the MS. The tilde represents ideal sensor data free from noise.

Sensor noise of Xsens MTi-G-700 was characterized by an Allan variance analysis [3]-[5]. With these noise characteristics white noise and Gauss-Markov processes were generated and superimposed to the sensor data resulting in representative real-world sensor data sequences $\mathbf{a}(t)$ and $\boldsymbol{\omega}(t)$.

The WiFi error model is based on an experimentally verified 1D-simulation, where several time-delay estimation algorithms were evaluated under different frequency-selective channel parameters, i.e. delay spread, coherence bandwidth and Rician K-factor. The mean location error

$$\mathrm{MLE} = \sqrt{(s_x - \Delta s_x)^2 + (s_y - \Delta s_y)^2 + (s_z - \Delta s_z)^2} \tag{1}$$

served as quality measure for the location accuracy, in which Δs_x, Δs_y and Δs_z denote single path errors in x/y/z-directions, respectively. The MLE was determined using least squares TDOA location schemes. Hence, MLEs are e.g. 7.5 m for g-std, 2.75 m for n-std and 0.95 m for ac-std using MUSIC TDOA as time-delay estimators [1][2]. By adding AWGN (Additive White Gaussian Noise) to WiFi range estimations the data sequence $\mathbf{p}(t)$ is produced representing noisy WiFi position information.

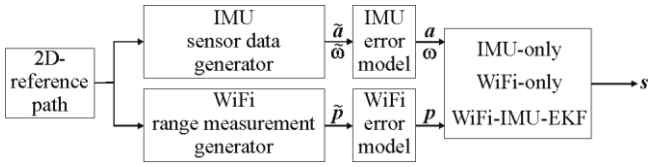

Fig. 1. Simulation model.

The noise-corrupted data $\mathbf{a}(t)$, $\boldsymbol{\omega}(t)$ and $\mathbf{p}(t)$ are then fed into the WiFi-IMU-EKF navigation algorithm. To evaluate the WiFi-IMU-EKF performance also the WiFi-only and IMU-only solutions were calculated.

V. Simulation Results

The 2D-reference path taken for the simulation is shown in both curves of Fig. 2 by the black dashed line. Starting from point A (0 m, 0 m) the MS is in standstill for about 60 s at coordinates B (21.6 m, 44.3 m), C (−16.9 m, 40.8 m) and D (−6.4 m, 20.2 m), respectively. While navigation results of IMU-only and WiFi-IMU-EKF in n-std are given in the lower curve of Fig. 2 by the grey solid line and the black solid line, respectively, the n-std WiFi-only curve is displayed in the upper curve. Especially in standstill phases of the MS, i.e. MS is at points B, C and D, location error (LE) increases for IMU-only due to position instabilities. IMU-only exhibits a LE ≈ 10 m at the end of the simulation run. With an external navigation reference, here a WiFi-IMU-EKF navigation algorithm, the position estimation will improve significantly, where LE of WiFi-IMU-EKF is 0.1 m at the end of the simulation.

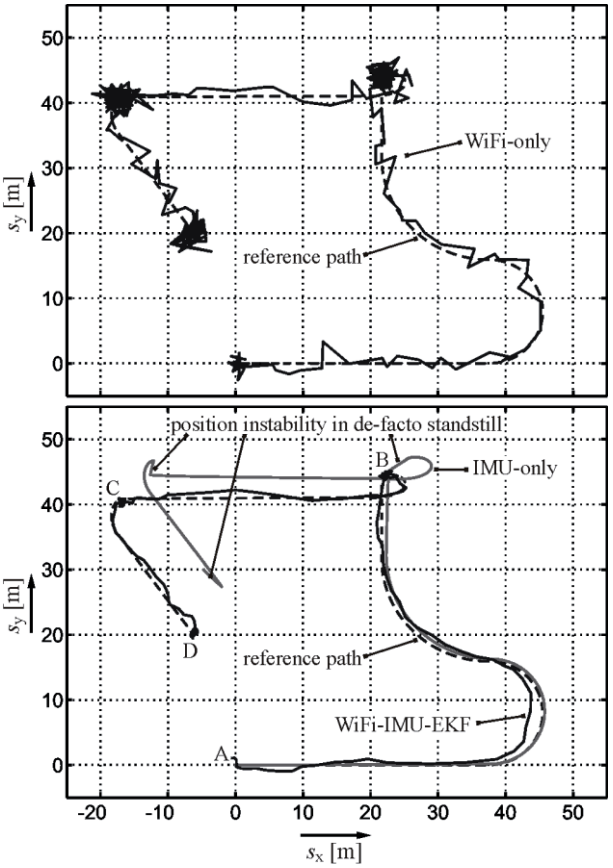

Fig. 2. Performance comparison of the n-std WiFi-only in the upper curve and n-std WiFi-IMU-EKF and IMU-only navigation filter in the lower curve.

The IMU-only, n-std WiFi-only and n-std WiFi-IMU-EKF LEs as a function of time t are given in the lower curves of Fig. 3. The motion state of the MS is sketched in the upper curve. Here '0' represents standstill and a '1' denotes motion. Thus the vertical lines define the transition from moving to standstill. As can be seen, in the IMU-only solution the

ISBN 978-3-8007-3585-3

position instability in standstill produces a large LE increasing in the course of time. While a LE decrease for WiFi-only is not visible in true MS standstill, LE typically converges towards 0 for WiFi-IMU-EKF within a few seconds as can be seen at t = 150 s.

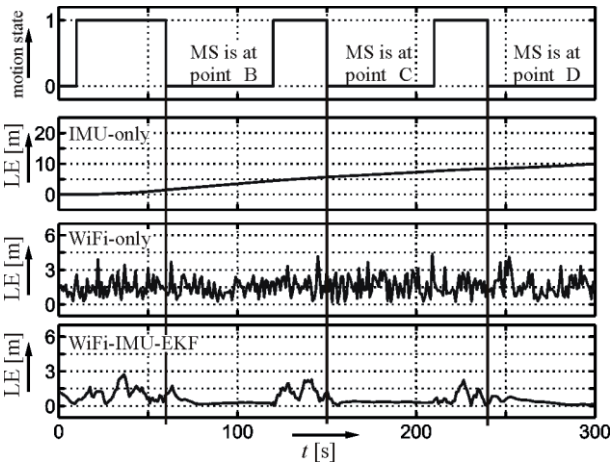

Fig. 3. True MS motion state (upper curve) and location error (LE) of IMU-only, WiFi-only and WiFi-IMU-EKF solution.

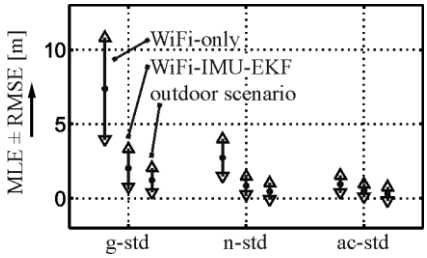

Fig. 4. Reducing mean location error (MLE) and root mean square error (RMSE) by using WiFi-IMU-EKF compared to WiFi-only navigation filter in g/n/ac-std.

The WiFi-IMU-EKF-based improvement in location accuracy is depicted in Fig. 4. Here, the WiFi-only and WiFi-IMU-EKF performance behavior for g/n/ac-std has been evaluated for $300\,\mathrm{s} \cdot 100\,\mathrm{Hz} = 30000$ estimated positions. Furthermore, the results of the WiFi-IMU-EKF approach in an ideal outdoor scenario are depicted, where an electromagnetic wave propagation without multipath effects has been assumed. For each simulation run the MLE and the root mean square error (RMSE) has been evaluated. MLE and RMSE are displayed from the left to the right with three vertical lines representing the results of WiFi-only, WiFi-IMU-EKF and the outdoor scenario, respectively. As can be seen WiFi-IMU-EKF MLE has been reduced at least by a factor of 2. While WiFi-IMU-EKF exhibits 2.04 m, 0.86 m and 0.52 m for the MLES for the g/n/ac-stds, WiFi-only delivers MLEs of 7.38 m, 2.73 m and 0.96 m, respectively. The outdoor scenario produces MLEs of 1.22 m, 0.47 m and 0.30 m for the g/n/ac-stds. Also a strong decrease for the RMSEs can be noticed for the WiFi-IMU-EKF navigation filter.

In order to test the WiFi-IMU-EKF navigation filter under aspects of initial position error and its error convergence following scenario was assumed. The initial position error is set to $\Delta s_x = -2.5$ m and $\Delta s_y = 5.5$ m resulting in a LE ≈ 6 m at the starting point A. As can be seen in Fig. 5 the position converges to the reference path rapidly within 3 s after a 10 s lasting standstill phase at coordinate A. Then the WiFi-IMU-EKF estimated position merges with the 2D-reference path.

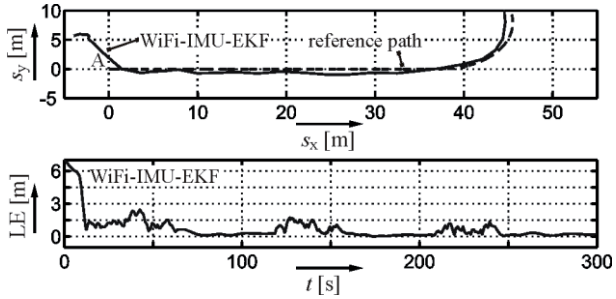

Fig. 5. WiFi-IMU-EKF error convergence after initial position error.

VI. Conclusion

This paper proposed an integrated WiFi-IMU-EKF navigation algorithm using time-delay estimation algorithms and MS motion state information delivered by inertial sensors. For performance evaluation WiFi range estimates and IMU sensor data were generated based on a 2D-reference path and a noise error model. The noise corrupted measurement data served as input for the WiFi-IMU-EKF, WiFi-only and IMU-only navigation algorithms. Simulation results illustrate the improvement of location accuracy for the WiFi-IMU-EKF navigation filter combined with an improvement in robustness against initial position error compared to conventional solutions. E.g. n-std WiFi-IMU-EKF LE is about one third compared to WiFi-only LE.

References

[1] K. Keunecke, and G. Scholl, "Wi-Fi-Based Performance Analysis of TOA/TDOA Estimators by Stochastic Channel Simulations" IEEE International Symposium on Wireless Communication Systems, Ilmenau, Germany, Aug., 2013.

[2] K. Keunecke, and G. Scholl, "Deriving 2D TOA/TDOA IEEE 802.11 g/n/ac Location Accuracy From An Experimentally Verified Fading Channel Model," IEEE International Conference on Indoor Positioning and Indoor Navigation, Montbeliard, France, Oct. 2013

[3] K. Keunecke, and G. Scholl, "Bewegungszustandsbestimmung ungestützer MEMS-Beschleunigungssensoren," tm - Technisches Messen, Oldenbourg Wissenschaftsverlag, 4/2013, Apr. 2013.

[4] K. Keunecke, and G. Scholl, "Motion State Prediction by Unaided Inertial Micor-Machined Accelerometers," SENSOR+TEST 2013, Nürnberg, May, 2013.

[5] K. Keunecke, and G. Scholl, "Reducing Position Instability of Unaided Inertial Navigation Systems in Standstill," IEEE Conference on Emerging Technologies and Factory Automation, Cagliari, Sep., 2013.

[6] G. Savage, Strapdown analytics. Maple Plain, Minnesota: Strapdown Associates Inc., 2007, vol. 2.

[7] E. von Hinüber, "Bahn- und Positionsvermessung von Industrierobotern mit inertialen Messystemen" PhD thesis, University of Saarbrücken, 1993.

[8] G. Welch, and G. Bishop, "An Introduction to the Kalman Filter," University of North Carolina at Chapel Hill, 2001.

[9] R.G. Brown, and P.Y.C. Grover, Introducing to Random Signals and Applied Kalman Filtering. John Wiley & Sons, 3rd ed., New York, 1997.

[10] Xsens, MTi 100-series. The most accurate and complete MEMS AHRS and GPS/INS. 2005-2012.

ISBN 978-3-8007-3585-3